Intercalate structure, melting, and the commensurate-incommensurate transition in bromine-intercalated graphite

A. Erbil,* A. R. Kortan, and R. J. Birgeneau
Department of Physics, Massachusetts Institute of Technology, Cambridge, Massachusetts 02139

M. S. Dresselhaus
Department of Electrical Engineering and Computer Science and Center for Materials Science and Engineering, Massachusetts Institute of Technology, Cambridge, Massachusetts 02139

(Received 28 April 1983)

In situ high-resolution x-ray scattering experiments have been carried out to study in-plane intercalate structure and phase transitions as a function of temperature in a single crystal graphite host. For the case of bromine-intercalated graphite the intercalate plane has three sublattices and each sublattice has a centered $(\sqrt{3}\times 7)$ rectangular structure with four Br_2 molecules per two-dimensional unit cell in the commensurate phase. The coherently ordered in-plane bromine regions exceed 10 000 Å in size. Above the commensurate-incommensurate transition (342.20±0.05 K), a stripe domain phase becomes established in a single domain of a sublattice along the sevenfold direction. The incommensurability as a function of reduced temperature exhibits a power law with an exponent of 0.50±0.02, confirming the existing theories. The relative shifts observed for the various harmonics are accurately predicted by a sharp-domain-wall model with $4\pi/7$ phase shifts. A power-law line shape is observed for the incommensurate intercalate layer, yielding values for the exponent η consistent with model calculations. Results on the temperature dependence of the intensities, linewidths, and line shapes of several Bragg peaks around the melting transition are presented. The intercalate layer exhibits a continuous melting transition from a two-dimensional solid phase to an anisotropic fluid phase, occurring at 373.41±0.10 K for a stage-4 compound.

I. INTRODUCTION

Phase transitions in two-dimensional (2D) systems have been the subject of intensive study motivated both by experimental observations and by intrinsic theoretical challenges.[1] Among the most interesting transitions taking place in two dimensions are commensurate-incommensurate[2–4] and melting transitions.[5] Perhaps the simplest realization of such systems have been rare-gas monolayers physisorbed onto the (00*l*) basal plane of graphite.[6–8] Another important class of 2D, or more accurately quasi-2D, materials is graphite intercalation compounds.[9]

Graphite intercalation compounds are layered compounds of graphite which are formed by the insertion of atomic and molecular layers that are periodically arranged in a matrix of graphite layers. Graphite intercalation compounds[9] are thus classified by a stage index n denoting the number of graphite layers between adjacent intercalate layers.

The types of ordering prevalent in graphite intercalation compounds include staging, stacking order of the graphite layers, in-plane ordering in the graphite and intercalate layers as well as interlayer correlations between these layers, commensurate and incommensurate molecular ordering, and interlayer intercalate stacking order. The intercalation compounds occur in highly anisotropic layered structures where the intraplanar binding forces are large in comparison with the interplanar binding forces. Therefore, the transitions between the ordered phases may provide good examples of phase transitions in quasi-one- and -two-dimensional systems.

Br_2-intercalated graphite compounds are particularly interesting because of the existence of several structural orderings in the intercalate bromine layers and the occurrence of phase transitions between these ordered phases.[10,11] The types of in-plane orderings prevalent in Br_2-intercalated graphite compounds are commensurate, incommensurate, and fluid phases. Several independent experiments on Br_2-intercalated graphite compounds exhibit anomalous temperature-dependent behavior above room temperature. X-ray diffraction[11] from the *a* face of a desorbed Br_2-intercalated graphite compound has provided evidence for the existence of a commensurate-incommensurate transition (CIT) at approximately 340 K, in addition to a melting transition at 373.7 K in the intercalate layer. The temperature dependence of the Raman line shape, linewidth, frequency, and intensity of the intercalate bromine molecular stretch mode[12] of Br_2-intercalated graphite compounds has yielded information on the CIT and melting transitions, consistent with these x-ray experiments.

X-ray diffraction has proven[6,13–15] to be an extremely useful probe of the structures and phase transitions in 2D systems. Not only can the crystal symmetry and lattice constants be deduced, but detailed line shape analysis can yield information about the extent and form of the interplanar and intraplanar correlations. Therefore, x-ray

scattering was chosen to study quantitatively the nature of the phase transitions in Br_2-intercalated graphite compounds.

Following the pioneering work of Frank and van der Merwe,[16] a large number of theories have been constructed for the CIT based on the domain-wall model.[3,17,18] These theories model the incommensurate phase by locally commensurate regions separated by sharp domain walls in which the structure shifts from one sublattice to another. The CIT then involves the spontaneous generation of domain walls. These theories are most complete for one-dimensional (1D) domain walls in a 2D lattice; that is, for a 2D system which exhibits a CIT in only one direction. This structure is called a stripe domain phase.

Frank and van der Merwe[16] considered a model where an array of atoms connected with harmonic springs interact with a sinusoidal substrate potential. Treating the adatom positions as a continuous variable, they predicted a certain critical amount of misfit below which the monolayer is in the commensurate state and above which the monolayer is in an incommensurate state described by the domain-wall model. McMillan[19] used a phenomenological Ginzburg-Landau free energy to treat the CIT in the layered compound $TaSe_2$. Considering only phase fluctuations in the order parameter, McMillan[19] obtained a free energy identical to the Frank and van der Merwe model and solved it numerically. Later, Bak and Emery[20] solved McMillan's model analytically, again rederiving the exact solution of Frank and van der Merwe.

Pokrovsky and Talapov[3,21] investigated the stripe domain phase by generalizing the Frank and van der Merwe model into two dimensions and found a continuous CIT. They predicted that for this system at finite temperatures the domain-wall density, that is, the number of domain walls per unit length, should exhibit the simple behavior $\rho \sim (T-T_c)^{\beta}$ with $\beta=0.5$. Fisher and Fisher[18] studied the effect of the fluctuation-induced wandering of the domain walls on the nature of the uniaxial CIT in a d-dimensional system and found $\beta=(3-d)/2(d-1)$ in agreement with Pokrovsky and Talapov for $d=2$. Moncton *et al.*[14,22] first provided strong experimental evidence that the 2D hexagonal-hexagonal CIT for low-order commensurate systems is, in fact, a melting transition. Following this, Coppersmith *et al.*[23] and Villain *et al.*[24] predicted that in the stripe domain case the CIT should also be a melting transition for commensurability $p<2\sqrt{2}$, where p is the ratio of the superlattice period to the underlying lattice period. For $p<2\sqrt{2}$, the domain walls are not stable to the spontaneous creation of dislocations in the stripe domain phase. Only for $p>2\sqrt{2}$ should one have a solid-solid transition with the incommensurability simply related to the domain-wall density.[23,24]

It has been shown by many theoretical studies[3,4,23,25,26] that there is no long-range order in 2D incommensurate solids. Instead, the 2D incommensurate phase is a floating phase with an algebraic decay of the positional correlation function. In these systems the long-range order is destroyed by the existence of a Goldstone mode with divergent amplitude, and therefore one anticipates $q^{-2+\eta}$ power-law singularities rather than true Bragg peaks. In the incommensurate phase, the Goldstone mode corresponds to the acoustic branch of the domain-wall lattice. For a commensurate system, the phonon spectrum has a gap at $q=0$; therefore there are Bragg singularities limited only by the finite size. Shultz[26] calculated the correlation function of domain walls in a stripe domain phase for $2\pi/d$ phase slips by using a fermion description and found an anisotropic XY model with $\eta_{G_0}=2/d^2$, where G_0 is the smallest reciprocal-lattice vector in the incommensurate direction. The incommensurate Br_2 layer may be an ideal system to test these predictions, because in this system the domain-wall structure in the incommensurate phase is well understood.

The nature of the solid-fluid transition in 2D incommensurate solids has been under intense investigation in recent years.[5,27,28] Kosterlitz and Thouless[27] first suggested the possibility of a continuous melting transition mediated by dislocation unbinding. A high-resolution synchrotron x-ray scattering study of xenon on graphite by Heiney *et al.*[6] revealed a continuous melting transition consistent with the theory of dislocation-mediated melting. Ostlund and Halperin[28] considered the dislocation-mediated melting of anisotropic layers of molecules and, depending on the symmetry of the Burgers vector of the dislocation, they predicted 2D solidlike, 2D smecticlike, 2D nematiclike, and quasi-isotropic behavior. The graphite-Br_2 system appears to be an ideal system for testing these theories of anisotropic 2D melting, since the 2D bromine lattice is highly anisotropic and it becomes incommensurate only in one direction.

In this paper, the results of an extensive x-ray scattering study of the phase transitions in stage-4 bromine-intercalated graphite, $C_{28}Br_2$, are presented. The stage-4 compound was chosen for study because of its weak interplanar interaction and resulting quasi-2D behavior. The format of this paper is as follows. In Sec. II we describe the experimental techniques; Sec. III presents the results on the structure of the commensurate phase. Also in Sec. III, we describe the measurement of the intercalate domain size and the kinetics of the intercalation process. Section IV gives the results on the CIT in the graphite-Br_2 system. In Sec. V we describe the Br_2 layer in the incommensurate phase and discuss its behavior in terms of current theories of continuous symmetry 2D solids. Section VI gives the results on the melting of the incommensurate Br_2 layer. A preliminary account of the CIT experiments and their analysis was given in Ref. 10.

II. EXPERIMENTAL DETAILS

Kish graphite single crystals of very high quality were used in these experiments. The samples, which had typical sizes of $2\times1\times0.1$ mm^3, were intercalated *in situ* on the x-ray spectrometer by a vapor transport technique[29] in a Pyrex chamber. The system for the *in situ* experiment is shown in Fig. 1. Two separate two-stage ovens were used to control the temperature of the sample and of the pristine bromine, independently. The sample was glued to a nickel block from its c face by using a minute amount of

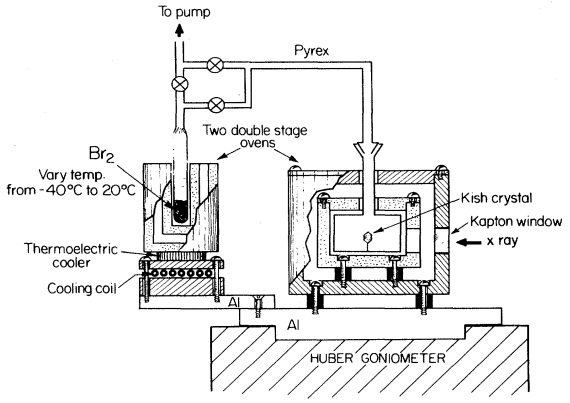

FIG. 1. Experimental arrangement for the *in situ* x-ray experiment.

bromine-resistant epoxy as shown in the inset of Fig. 2. There was no observable epoxy-induced strain in the crystal before and after the intercalation. This is due to the fact that the crystal expands only in the c direction during intercalation. The temperature measurements were made by attaching a precision thermistor to the nickel block. The temperature stability of the sample was adequate for these studies; the temperature drift was about 5 mK in 4 h. After intercalation to stage 4, the bromine pressure was kept constant at 57 Torr (bromine temperature was -3 °C) during subsequent measurements to ensure chemical stability.

The experiments were carried out on a three-axis x-ray spectrometer with the use of Mo$K\alpha$ ($\lambda=0.7107$ Å) radiation from a Rigaku 12-kW rotating anode x-ray source. Figure 2 gives a schematic representation of the experimental arrangement. The x-ray beam is collimated by successive slits S_1, S_2, and S_3 before the sample and slit S_4 after the sample. For most of the measurements, pyrolytic graphite crystals were used as monochromator and analyzer. The longitudinal resolution was 1.7×10^{-2} Å^{-1} halfwidth at half-maximum (HWHM) and the transverse in-plane resolution was 1.4×10^{-3} Å^{-1} HWHM at $q=1.45$ Å^{-1}. For the measurements of the intrinsic

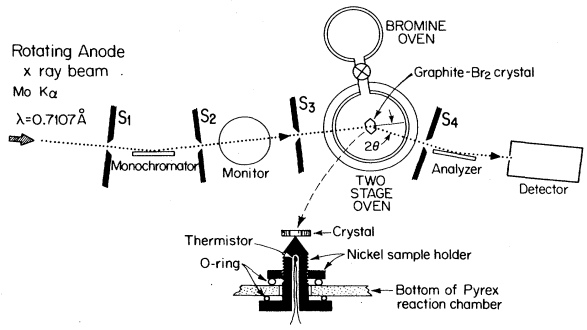

FIG. 2. Schematic diagram of the x-ray spectrometer. Inset shows the details of the bromine-intercalated graphite sample holder.

domain sizes, Ge(111) crystals were employed as monochromator and analyzer. This latter configuration yields more than an order of magnitude improvement in the resolution.

III. STRUCTURE OF COMMENSURATE PHASE

A. Out-of-plane ordering

Figure 3 shows a typical θ—2θ scan in the (00l) direction taken for stage determination. The inset of Fig. 3 gives the details of the scattering configuration. All of the (00l) peaks observed can be indexed on the basis of reflections from a stage-4 bromine-intercalated graphite compound. The c axis repeat distance I_c is $I_c=c=17.07\pm0.01$ Å, in agreement with previous measurements.[29] In a stage-4 compound, there are four graphite layers between two adjacent intercalate layers.

Interlayer correlations between the bromine intercalate layers have been studied via the (0kl) reflections. Figure 4(a) indicates reciprocal-lattice points in the $h=0$ plane. The reciprocal-lattice points which have contributions from both bromine and carbon correspond to true three-dimensional (3D) peaks (triangles). The pure bromine superlattice points (solid circles) exhibit Bragg rods rather than points in reciprocal space. The rods, which are oriented in the l direction, indicate the absence of long-range order in the c direction in real space. To demonstrate this point, we performed scans along the Bragg rods passing through the in-plane peaks Br(0,4,0) at $k=1.455$ Å^{-1} and Br(0,6,0) at $k=2.185$ Å^{-1}, which are respectively labeled in Fig. 4(a) as B and A. Figures 4(b) and 4(c) show the data obtained at room temperature for scans B and A, respectively. The solid lines are fits of the scattered intensity to a constant plus sinusoidal l dependence, corrected for the increasing scattering volume with increasing l. At room temperature the rods show about 30% sinusoidal modulation due to the correlations between nearest intercalate planes. It is of significance to note that these scans

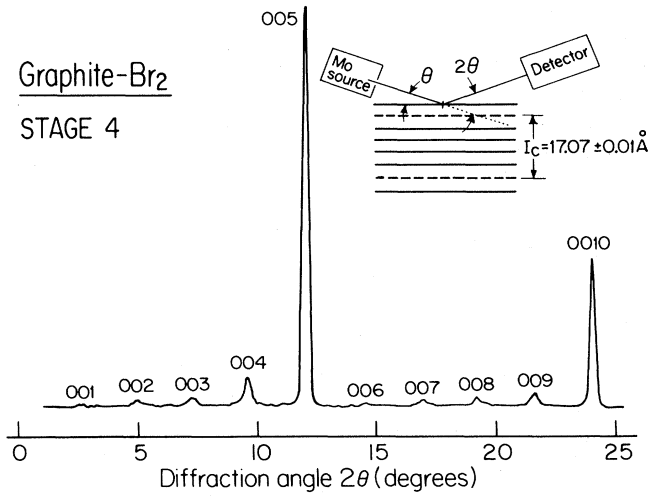

FIG. 3. θ—2θ scan taken for stage determination. Inset gives the details of the scattering configuration for the (00l) scans.

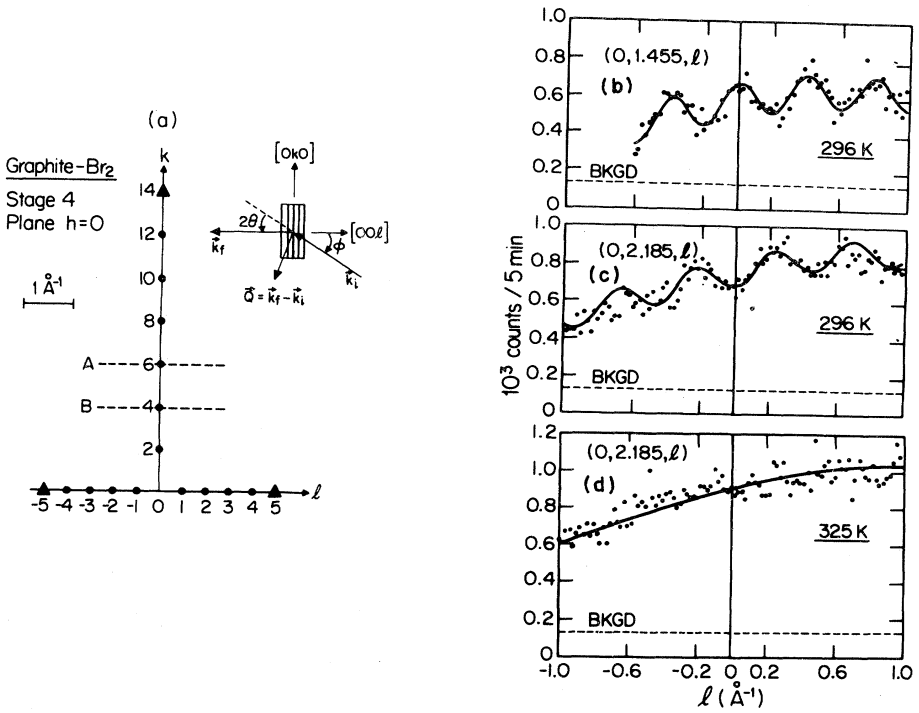

FIG. 4. (a) Reciprocal plane $h=0$. The reciprocal-lattice points which have contributions from both bromine and carbon correspond to true 3D peaks (triangles). The pure bromine superlattice points (solid circles) exhibit Bragg rods rather than points in reciprocal space. Inset shows the scattering geometry. (b) Scan at $T=296$ K along the Bragg rod passing through the in-plane peak Br(0,4,0) at $k=1.455$ Å^{-1} which is labeled as A in (a). (c) Scan at $T=296$ K along the Bragg rod passing through the in-plane peak Br(0,6,0) at $k=2.185$ Å^{-1}, which is labeled as B in (a). (d) Same as (c) but at $T=325$ K.

indicate the absence of long-range order at room temperature in the c direction. However, a partial correlation between nearest-neighbor intercalate planes is found. The periodicity of the Bragg rod modulation is 16 ± 2 Å, which is equal to I_c determined from $(00l)$ reflections within the error. However, as the temperature is raised to 325 K the modulation for scan A has vanished, as shown in Fig. 4(d). This indicates that at these higher temperatures the intercalate layers are completely uncorrelated and the Br_2 layer is essentially a 2D system.

Another important observation in Figs. 4(b) and 4(c) is that the phase of the sinusoidal modulation for the rod at $k=1.455$ Å^{-1} is shifted by $180°\pm20°$ with respect to the phase of the rod at $k=2.185$ Å^{-1}. This indicates that at room temperature one intercalate plane is translated by $(0.25\pm0.003)b$ with respect to the nearest-neighbor intercalate plane in the sevenfold direction, where b is the unit cell dimension in the sevenfold direction. In the commensurate phase, the closest possible translation to the value $(0.25\pm0.03)b$ in the sevenfold direction is $3b/14$ for the stacking arrangement *AIABABIB*. This expected translation due to stacking of the intercalate planes is close but slightly smaller than the measured value. Further work with a more intense x-ray source is needed to understand clearly the stacking arrangement in the bromine-intercalated graphite.

Correlations in the site ordering of the intercalant in sequential intercalate layer planes has also been observed in a number of compounds, particularly in stage-1 compounds.[30,31] Because of the relatively large size of the intercalant ions or molecules relative to the carbon atoms, the correlation of the site arrangement of the intercalant on sequential layers allows for closer packing of the intercalate layers in the 3D stacking of the crystal. Even when long-range correlation is absent, these close-packing considerations imply that the placement of the intercalant on a particular site on one layer tends to exclude the placement of the intercalant on a similar site in the nearest-neighbor intercalant layer.[30,31] It is of significance to note that at high temperatures in stage-4 bromine-intercalated graphite, even the correlation in the stacking of bromine intercalate layers disappears. To establish that we have true Bragg rods, we have performed several scans perpendicular to the Bragg rods. Figures 5(a) and 5(b) show the scans perpendicular to the Bragg rods passing through the in-plane peaks Br(0,4,0) and Br(0,6,0), respectively, at various l values. All these scans at various l values yielded the same line shape and linewidth within the error. The linewidth is resolution-limited for each Bragg rod, indicating the existence of long-range order in the plane. This should be contrasted with the absence of stacking site ordering along the c direction.

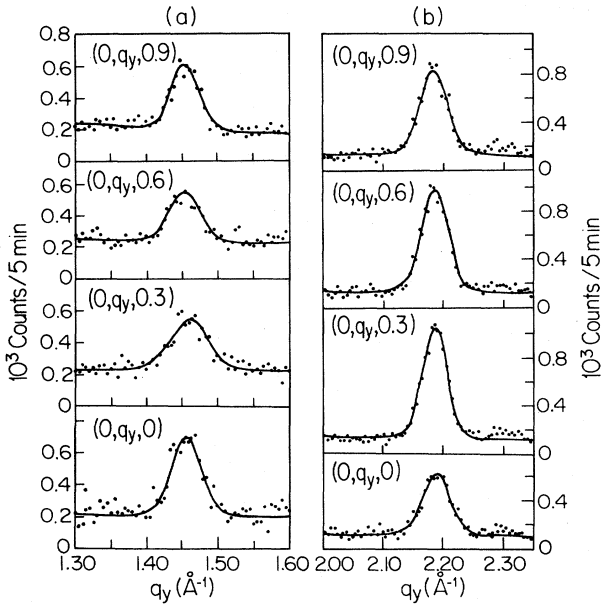

FIG. 5. Scans perpendicular to the Bragg rod passing through the in-plane peaks: (a) Br(0,4,0) at various l values, and (b) Br(0,6,0) at various l values.

B. In-plane structure

Information on the in-plane intercalate bromine arrangement is, of course, obtained by studying $(hk0)$ reflections. The Bragg spots in reciprocal space form three equivalent subsets corresponding to three equivalent sublattices in real space rotated by 120° with respect to each other. As will be described in Sec. III D, the size of each domain can be larger than 10 000 Å. The Br_2 layer structure is defined as one of the three rotationally distinct in-plane sublattices of the intercalate layer.

The observed in-plane reflections occur for $h+k=2n$, where n is an integer. We did not observe the additional in-plane reflections reported earlier.[32] The result $h+k=2n$ is an indication that the in-plane unit cell is face centered. We find, in agreement with others,[33] that at room temperature each Br_2 domain exhibits a centered $(\sqrt{3}\times 7)$ rectangular superlattice structure with four Br_2 molecules per 2D unit cell. This structure corresponds to a stoichiometry of $C_{7n}Br_2$, where n is the stage index, consistent with the determination from $(00l)$ reflections.[34] The sevenfold axis of the Br_2 unit cell is oriented along the [110] direction of the graphite lattice. Those reflections, which have indices k that are a multiple of 7, lie at the positions of the normal graphite $(hk0)$ reflections and their intensity is determined by the precise positions of the bromine atoms relative to the graphite layers as well as by the relative positions of the bromine atoms with respect to one another. The remaining h and k reflections which are superlattice peaks are sensitive only to the relative positions of the bromine atoms. We have used eight superlattice reflections to determine the in-plane atomic arrangement in a Br_2 unit cell as shown in Table I. This structure is quite close to that originally proposed by Eeles and Turnbull.[32]

TABLE I. Observed and calculated structure factors for in-plane Br_2 ordering in the commensurate phase.

h,k,l	$\lvert F^{\rm obs}\rvert$	$\lvert F^{\rm calc}\rvert$
0,2,0	5	22
0,4,0	56	56
0,6,0	88	88
0,10,0	44	48
0,12,0	19	26
1,1,0	51	53
1,3,0	26	24
1,5,0	27	29
1,9,0	29	36

The experimentally measured integrated intensities I_{hk0} were converted to structure factors $F^{\rm obs}_{hk0}$ using the relation

$$I^{\rm obs}_{hk0}=SC_LC_AC_g\,|F^{\rm obs}_{hk0}|^2\,, \tag{1}$$

where S is a scale factor and C_L is the combined Lorentz and polarization correction, which for nonpolarized radiation takes the form $C_L=[1+\cos^2(2\theta)]/\sin(2\theta)$. The absorption coefficient C_A has a very small angular dependence in the transmission configuration for a small sample; therefore, we can neglect this correction. The factor C_g is necessary to correct for the absorption by the glass ampoule, but because the ampoule is cylindrical, we can also neglect the angular dependence of this correction for $(hk0)$ reflections.

The structure factor $F^{\rm calc}_{hk0}$ is given by the sum of the diffracted amplitudes contributed by each of the atoms in the unit cell,[35]

$$F^{\rm calc}_{hk0}=\sum_J f_J\exp(2\pi ihx_J+2\pi iky_J)\,, \tag{2}$$

and contains information on the structure projected onto the xy plane. Here (x_J,y_J) denotes the coordinates of the Jth atom within the unit cell. The scattering factor for bromine atom J is given by

$$f_J=f^0_J\exp[-B_J(\sin^2\theta)/\lambda^2]\,, \tag{3}$$

where f^0_J is the scattering factor for a bromine atom at rest, and B_J is the Debye-Waller temperature factor. Table I lists the observed structure factors $F^{\rm obs}_{hk0}$ along with the corresponding calculated structure factor $F^{\rm calc}_{hk0}$ for a number of $(hk0)$ points. The standard measures used to assess the agreement between $F^{\rm calc}_{hk0}$ and $F^{\rm obs}_{hk0}$ are the residual[36] or the weighted residual,[37]

$$R_w=\left[\sum w(\,|F^{\rm obs}|-|F^{\rm calc}|\,)^2\Big/\sum w\,|F^{\rm obs}|^2\right]^{1/2}\,, \tag{4}$$

where w is a weight defined for each observation in terms of the structure factor variance σ^2, such that $w=\sigma^{-2}$. The residual R and the weighted residual R_w for the structure are 0.12 and 0.05, respectively. The calculated structure factors were based on the coordinates given in Table II with four nonzero coordinates as adjustable parameters

TABLE II. Bromine atom positions in a base in the commensurate phase. Positions are given in the units of the centered $(\sqrt{3}\times 7)$ unit-cell lattice vectors.

J	x_J	y_J
1	0	0
2	0	0.13
3	0	0.32
4	0.5	0.31

during the least-squares fit and an isotropic Debye-Waller factor $B=5.5$ Å^2 as given in an earlier work.[32] We also used the least-squares structure refinement program RFINE4 (Ref. 38) to obtain more precise values for the structural parameters; however, the analysis yielded parameters not significantly different from the ones given earlier.[32]

The structure determination is approximate because of the limited number of reflections used. Further studies employing more $(hk0)$ and (hkl) reflections are needed to determine the precise molecular arrangement in the unit cell. The areas per Br_2 molecule are, respectively, 18.33 and 19.53 Å^2 in the intercalate Br_2 layer and in the pristine Br_2 layer.[39] It is interesting to note that the intercalate Br_2 layer is denser than the pristine bromine layer in the commensurate phase. This fact and the small Br-Br distances (2.14 and 2.24 Å) for the intercalate Br_2 suggest that the Br_2 molecules are tilted with respect to the plane. Assuming that the intercalate Br—Br bond length is 2.27 Å, which is the bond length for bromine molecules in the solid phase, then we expect tilt angles of 21° and 13° for the intercalate Br_2 molecules. Recent extended x-ray absorption fine-structure (EXAFS) measurements on a Br_2-intercalated highly oriented pyrolytic graphite (HOPG) indicates a tilting of the Br_2 molecules by a similar amount.[40] A phase with tilted Br_2 molecules is also observed in bromine molecules adsorbed on graphite.[41] The graphite-bromine-graphite sandwich thickness in the Br_2-intercalated graphite compound is 7.0 Å, which is large enough to accommodate a small tilt in the molecule. Figure 6 shows the in-plane intercalate Br_2 unit cell and the atomic arrangement in the extended lattice superimposed on the graphite lattice. Both the $(\sqrt{3}\times 7)$ rectangular unit cell and the primitive unit cell are shown in Fig. 6. By comparing our calculated structure factor and the experimental intensities, we can clearly rule out the $C_{14n}Br_2$ structure[42] in favor of the $C_{7n}Br_2$ structure for the samples used in the present work. This interpretation is consistent with the work on similarly prepared samples by Leung *et al.*[34] to determine the in-plane density of the intercalate layer, where the stoichiometry $C_{(7\pm 2)n}Br_2$ was obtained. There is no direct information on the relative positions of the bromine and carbon atoms. However, an earlier observation[43] by EXAFS indicates the Br atoms have a tendency to be situated close to the center of a basal-plane hexagon.

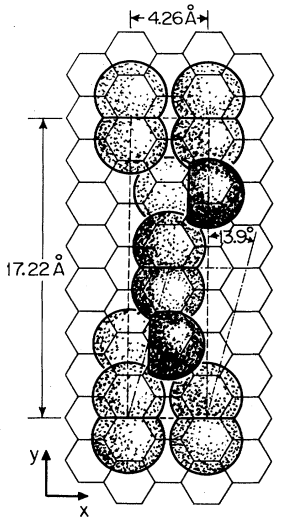

FIG. 6. This figure is similar to Fig. 1 of Ref. 10 except that the Br_2 molecules are drawn more closely to scale. Rectangular in-plane intercalate Br_2 unit cell (dashed lines) and the atomic arrangement in the lattice superimposed on the graphite lattice. Dashed-dotted line show the primitive unit cell.

C. Kinetics of bromine intercalation in graphite

We have investigated the Br(0,6,0) Bragg peak as a function of time to probe the kinetics of Br_2 intercalation into single-crystal Kish graphite. The scans through the Br(0,6,0) peak position taken at various times after the introduction of Br_2 gas are shown in Fig. 7. After 4 h, no

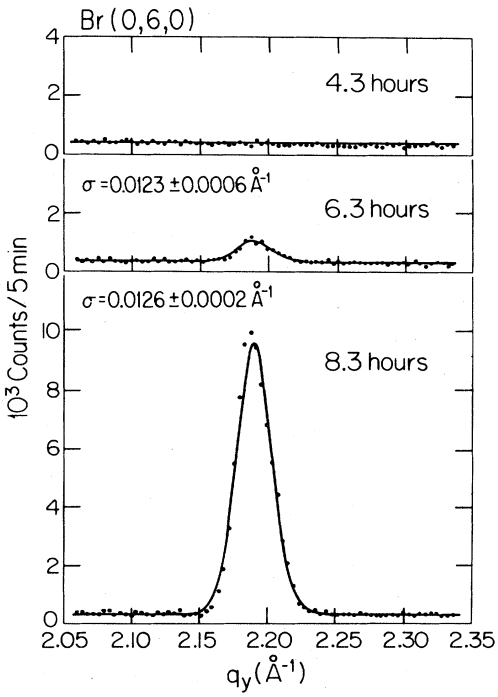

FIG. 7. Scans through the Br(0,6,0) peak position taken at various times after the initiation of intercalation. Solid lines are the results of fits by resolution-limited Gaussians.

Bragg peak nor diffuse background appeared, indicating that no intercalation had taken place. However, after 330 min, the Br(0,6,0) Bragg peak grows very rapidly, indicating the start of intercalation. Figure 8 shows the integrated intensity of the Br(0,6,0) peak as a function of time during the intercalation process. The absence of intensity until $t=330$ min may be interpreted to imply either that the intercalation process has not yet not started or that the intercalated Br_2 molecules are completely disordered in the graphite matrix. The absence of any observable change in the background scattering implies the absence of disordered intercalant. We further note that by $t\sim 800$ min, the integrated intensity of the Br(0,6,0) Bragg peak reaches its saturation value. These observations provide evidence that the majority of the intercalated Br_2 molecules form ordered intercalate domains.

Another important feature in Fig. 7 is the observation that the linewidth remains resolution-limited throughout the intercalation process, although the integrated intensity increases with time. This provides evidence that large domain sizes are formed starting with the initiation of intercalation. Because the experiments in this section are performed using a graphite monochromator and analyzer, we place a lower limit of 2000 Å for the average domain size during intercalation. It is conceivable that these domains are as large as the domains of saturated stage-4 compounds as discussed in the next section.

D. Measurement of in-plane domain size

For the measurement of the intrinsic Br_2 in-plane domain sizes, Ge(111) crystals were employed as monochromator and analyzer in the W configuration.[44] We have measured the resolution function of the nondispersive configuration by a reflection from a Si(111) crystal at the sample position. By scaling the measured resolution function to Br_2 superlattice peaks, we show that although the width of the longitudinal scan is resolution limited, the transverse scan has some finite-size broadening, in addition to the linewidth contribution from the mosaic spread. The finite-size contribution to the transverse HWHM of the Br(0,4,0) peak is of the order of 0.0003 Å^{-1}, which corresponds to an intercalate bromine domain size larger than 1 μm in the commensurate phase. This is the largest in-plane domain size reported in an intercalation compound and is consistent with the prediction of the domain sizes by Safran and Hamann[45] for systems not constrained kinetically. There is no observable change in the linewidth with increasing temperature until the CIT temperature $T_c=342.20$ K.

Figures 9(a) and 9(b) show the longitudinal scans of Bragg peaks agg peaks nd Br(0,6,0), respectively, in the commensuratmmensurat) and incommensurate (342.82 K) phases. We ases. We e only the peak widths since the peak positiorak positiorsities will be discussed in Sec. IV B. As shown in Fig. 9 there is a broadening in the linewidth in the incommensurate direction for the bromine superlattice peaks Br(0,4,0) and Br(0,6,0). In addition, the linewidth broadening is related to the incommensurability, giving larger broadening to the Br(0,6,0) peak due to the larger exponent η for this peak as will be discussed in Sec. V. Also, the distribution of chemical potentials for domain-wall formation may contribute to the linewidth very close to T_c. Figure 10 shows the transverse scans of the peak Br(0,6,0) in the commensurate and incommensurate phases, which provide evidence that even in the incommensurate state the in-plane intercalate coherence size is more than 1 μm.

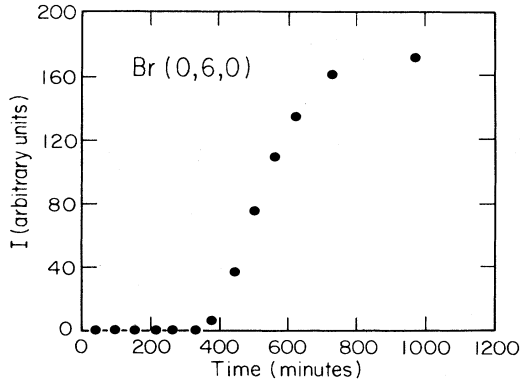

FIG. 8. Integrated intensity of the Br(0,6,0) peak as a function of time during the intercalation process.

IV. THE COMMENSURATE-INCOMMENSURATE TRANSITION

A. Theory

The Hamiltonian for an array of adatoms connected with harmonic springs in a cosine potential is given by

$$H=\sum_n\left[\frac{K}{2}(x_{n+1}-x_n-b_0)^2+V\left[1-\cos\left[\frac{2\pi}{a_0}x_n\right]\right]\right], \tag{5}$$

where x_n is the position of the nth atom, and K is the force constant between the adatoms. In the absence of the

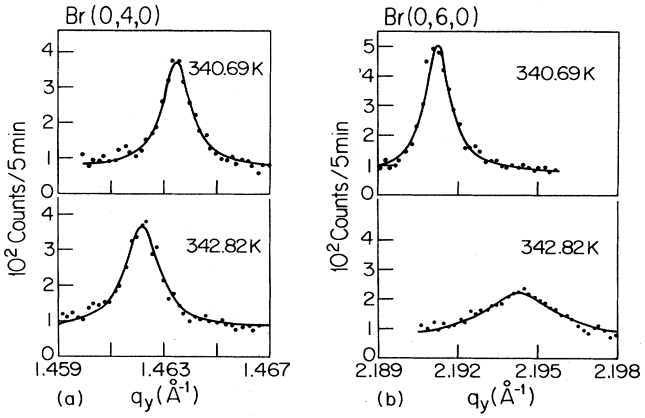

FIG. 9. Longitudinal scans of Bragg peaks (a) Br(0,4,0) and (b) Br(0,6,0) in the commensurate (340.69 K) and incommensurate (342.82 K) phases.

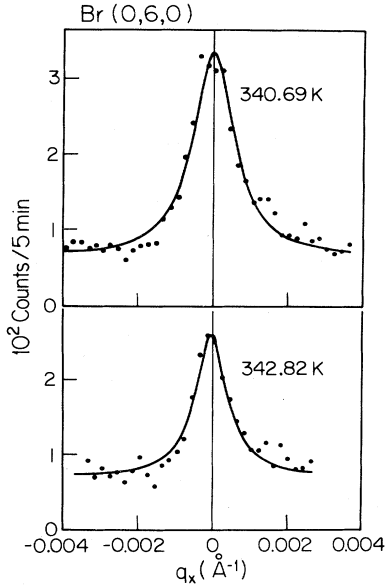

FIG. 10. Transverse scans of the Br(0,6,0) peak in the commensurate (340.69 K) and the incommensurate (342.82 K) phases.

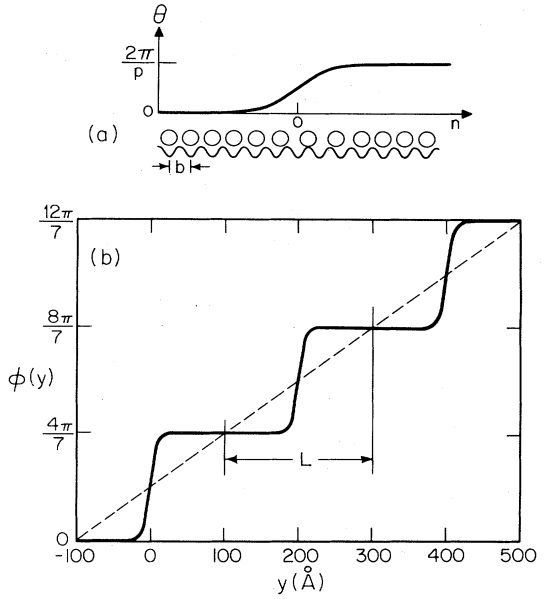

FIG. 11. (a) Single soliton solution of the sine-Gordon equation [Eq. (6)]. The soliton is a domain well between two commensurate regions. For the atomic arrangement shown above, $p=1$. (b) Soliton lattice solution to the sine-Gordon equation [Eq. (6)]. Straight line corresponds to the unperturbed adatom incommensurate structure. Flat regions correspond to the commensurate domains between the solitons. Solitons are separated by $L=200$ Å and the thickness parameter $L_0=5$ Å. Phase shift over a domain wall for bromine-intercalated graphite is $4\pi/7$.

periodic potential V, the harmonic term would favor a lattice constant b_0 which, in general, would be incommensurate with the substrate lattice constant pa_0, where p is a rational number. We assume that b_0 is very close to pa_0. The commensurate adatom lattice constant b is defined by $b=pa_0$. Introducing the phase $\phi(n)$ by the equation

$$x_n = nb + \frac{b}{2\pi}\phi(n) \tag{6}$$

and transforming to the continuum limit, the Hamiltonian becomes

$$H = \int \left[\frac{Kb^2}{8\pi^2} \left(\frac{d\phi}{dn} - \delta \right)^2 + V(1-\cos(p\phi)) \right] dn \ , \tag{7}$$

where

$$\delta = \frac{2\pi(b_0 - b)}{b} \tag{8}$$

is the misfit between the two lattices.

The state $\phi(n)=0$ is the commensurate state, and the unperturbed incommensurate phase ($V=0$) is given by the straight line $\phi(n)=\delta n$. Bak and Emery[20] observed that the function $\phi(n)$ for which the integral in Eq. (7) is a minimum will satisfy the sine-Gordon equation,

$$\frac{d^2\phi}{dn^2} = pA \sin(p\phi) \ , \tag{9}$$

one solution of which is the soliton $\Theta(n)$ or domain wall,

$$\phi(n) = \Theta(n) = \frac{4}{p} \tan^{-1} \exp(p\sqrt{A}\, n) \ . \tag{10}$$

This solution as shown in Fig. 11(a) describes a domain wall, centered at $n=0$, which separates two commensurate regions, one with $\phi=0$, the other with $\phi=2\pi/p$. The domain-wall width is

$$L_0 = \frac{1}{p\sqrt{A}} = \frac{b}{2\pi p}\sqrt{K/V} \ . \tag{11}$$

For large substrate interaction V, we expect sharp-domain walls, and this occurs for the case of bromine-intercalated graphite. In general, the solutions are regularly spaced domain walls with a lattice constant L [as shown in Fig. 11(b)] due to the repulsive interaction between them. These solutions have a functional form,

$$\phi(y) = \phi_0 + \frac{2\pi m}{p} + \Theta(y - mL) \ , \tag{12}$$

where m is the closest integer to y/L, $y=nb$, the function $\Theta(y)$ is defined in Eq. (10), and ϕ_0 is a constant. Later, we will use the phase function given in Eq. (12) to calculate the structure factor in a stripe domain phase.

The energy density of a regular array of domain walls with spacing L was calculated by Bak and Emery[20] as

$$E = \left[\frac{4\sqrt{A}}{\pi} - \delta \right] \frac{2\pi}{p}\rho + \frac{32\sqrt{A}}{p}\rho \exp\left[-\frac{p\sqrt{A}}{\rho} \right] , \tag{13}$$

where $\rho = 1/L$ is the domain-wall density. The first term in Eq. (13) is proportional to the domain-wall density ρ and may therefore be considered as the domain-wall ener-

gy. The second term decays exponentially with the distance between domain walls and thus represents an effective repulsion between the domain walls. When A becomes sufficiently small or δ sufficiently large so that the domain-wall energy becomes negative, the commensurate phase becomes unstable with respect to spontaneous formation of domain walls.

We may understand the existence of a CIT in Br_2-intercalated graphite at high temperature simply from the following argument. In the bromine-intercalated graphite compound, the graphite plane is very rigid, and therefore the in-plane unit-cell dimension does not change much with varying temperature. However, the intercalate Br_2 plane is very soft and anharmonic; therefore the increasing mismatch with increasing temperature drives the CIT at 342 K.

In the preceding calculations at $T=0$, fluctuations of the domain walls are completely neglected. Pokrovsky and Talapov[3,21] studied the stripe domain phase in 2D at finite temperatures. By using the connection between the quantum mechanics of a 1D system and the statistical mechanics of the 2D problem, they translated the problem into a fermion description. Here the coordinate along the domain wall (x axis) plays the role of the time. The motion of the domain wall in time in a 1D quantum system corresponds to bending of the domain walls in the 2D statistical system, and the fermion statistics ensure that the domain walls do not cross. In the quantum picture, domain walls have kinetic energy which should be added to the energy given in Eq. (13) to obtain the total energy density. The kinetic energy density for a fermion system in one dimension with density ρ is given by

$$E_{\rm kin}=\tfrac{1}{3}B\rho^3 , \tag{14}$$

where B is a constant. Thus the total energy density takes the form

$$E=(\delta-\delta_c)\rho+C\rho\exp(-D/\rho)+\tfrac{1}{3}B\rho^3 , \tag{15a}$$

where C and D are constants.

Close to the transition temperature the second term in Eq. (15a) can be neglected compared with the third term. In this case, the energy density in Eq. (15a) becomes

$$E\rightarrow(\delta-\delta_c)\rho+\tfrac{1}{3}B\rho^3 . \tag{15b}$$

Minimization with respect to ρ yields

$$\rho\sim(\delta_c-\delta)^{1/2} \tag{16a}$$

or

$$\rho\sim(T-T_c)^{1/2} . \tag{16b}$$

In Sec. IV B, the experimental results on the CIT will be compared to these theoretical results.

In scattering experiments the structure factor provides the medium for quantitative comparison between the experimental results and theoretical predictions. In Sec. III B, use of the structure factor for structure determination was discussed for the commensurate phase. Here we discuss the extra features introduced into the structure factor of the commensurate phase by the presence of a domain-wall lattice.

Because the CIT takes place only in one direction, we consider only the y direction. To simplify the formulas, we assume an atom with unit scattering intensity occupying each commensurate lattice point in the commensurate phase.

In the incommensurate phase the domain walls modulate the commensurate lattice. Let us consider explicitly the case where there is a net displacement of τ across each domain wall, with the walls occurring every N unit cells. We thence have a new unit cell of length $L=Nb+\tau$ with N atoms at positions y_n. The structure factor is then given by

$$S(q_y)=|f(q_y)|^2\delta\left[q_y-\alpha\frac{2\pi}{Nb+\tau}\right] , \tag{17}$$

where

$$f(q_y)=\sum_{n=1}^{N}e^{iq_y y_n} . \tag{18}$$

Here α is an integer and the δ function expresses the Bragg condition. Two limits are calculated in a straightforward manner. First, for uniform expansion, that is, for very broad walls, $f(q_y)=0$ unless α is an integral multiple of N. Second, for perfectly sharp-domain walls,

$$|f(q_y)|^2=\frac{\sin^2(Nbq_y/2)}{\sin^2(bq_y/2)} . \tag{19}$$

In this limit it is convenient to refer the incommensurate Bragg peak to the nearest commensurate position given by $q_y=k(2\pi/b)$; accordingly, we write

$$\alpha\frac{2\pi}{Nb+\tau}=k\frac{2\pi}{b}+\frac{2\pi}{L}\left[r-\frac{k}{p}\right] , \tag{20}$$

where k and $r=\alpha-kN$ are integers and $p=b/\tau$. It is straightforward to show that for Nb large, Eq. (19) simplifies to

$$|f(q_y)|^2=N^2\frac{\sin^2(\pi k/p)}{\pi^2[(k/p)-r]^2} , \tag{21}$$

so that

$$|f(q_y)|^2=\left|f\left[q_y-k\frac{2\pi}{b}\right]\right|^2 . \tag{22}$$

Henceforth we will use the notation $[h,(k,r),l]$ to denote the modulation peak r associated with the commensurate peak (h,k,l).

For the general domain-wall model,

$$y_n=(n-1)b+\frac{b}{2\pi}\Theta(n-N/2) , \tag{23}$$

where

$$\Theta(n-N/2)=\frac{4}{p}\tan^{-1}\exp[p\sqrt{A}\,b(n-N/2)] , \tag{24}$$

and

$$f(q_y)=\sum_{n=1}^{N}\exp\{iq_y[(n-1)b+(b/2\pi)\Theta(n-N/2)]\}\ . \tag{25}$$

To calculate relative intensities Eq. (25) must be evaluated numerically.

B. Results and discussions

We utilized the in-plane Bragg peak positions, intensities, linewidths, and line shapes to investigate the CIT in Br_2-intercalated graphite compounds. These parameters exhibit anomalous behavior across the CIT temperature. As the temperature is raised above 342.20 ± 0.05 K, the Br_2 Bragg rods shift along the q_y direction, simultaneously developing a composite line shape. To within an accuracy of 10^{-4} Å^{-1} the Br_2 Bragg rods shift only in one direction; namely, the system remains commensurate in the $\sqrt{3}$ direction (see Fig. 6).

Typical profiles in the sevenfold direction for the Br(1,5,0) and Br(0,6,0) peaks are shown in Fig. 12. The solid lines are all results of fits by Gaussians at the positions indicated by arrows. In the incommensurate phase for the Br(1,5,0) diffraction profile, the peak positions are at $q_y=5\tau_0-\frac{3}{2}\epsilon$ and $q_y=5\tau_0+2\epsilon$ as shown in Fig. 12(a), where ϵ is the temperature-dependent incommensurability for the principal component of the Br(0,6,0) peak. In the incommensurate phase for the Br(0,6,0) diffraction profile, the peak positions are at $q_y=6\tau_0-\frac{5}{2}\epsilon$ and $q_y=6\tau_0+\epsilon$ as shown in Fig. 12(b). The directions of the shifts of the principal components of the peaks around the commensurate positions are indicated by arrows in Fig. 13. Also, in Fig. 13 the peaks represented by the open circles, solid circles, and half-filled circles exhibit shifts of $\frac{1}{2}\epsilon$, ϵ, and $\frac{3}{2}\epsilon$, respectively, from their commensurate peak position during the CIT. It is evident that these q_y displacements cannot be understood on the basis of a uniform expansion or contraction of the intercalate lattice, since the principal Bragg peak positions are no longer low-order integral multiples of each other. This implies that the unit cell of the weakly incommensurate phase must be extremely large, suggesting a domain-wall or discommensuration model.

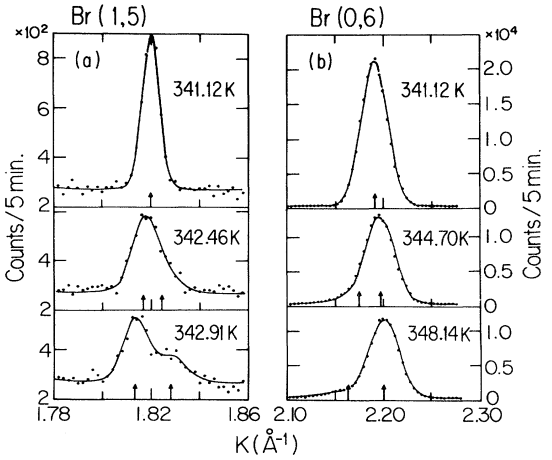

FIG. 12. (a) Br(1,5,0) diffraction profiles in the commensurate (341.12 K) and the incommensurate phases (342.46 and 342.91 K). (b) Br(0,6,0) diffraction profiles in the commensurate (341.12 K) and the incommensurate phases (344.70 and 348.14 K). Solid lines are all results of fits by resolution-limited Gaussians at the positions indicated by arrows.

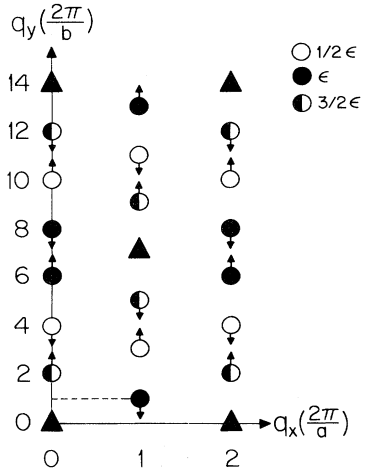

FIG. 13. Quadrant of the $l=0$ reciprocal plane of a Br_2 sublattice. Circles correspond to Bragg rods originating from the 2D Br_2 superlattice. Triangles represent 3D graphite and bromine peaks. Arrows at each Br_2 peak show the directions of the principal peak position shifts during the CIT. Bragg rods represented by the open circles, solid circles, and half-filled circles exhibit shifts of $\epsilon/2$, ϵ, and $3\epsilon/2$, respectively, from their commensurate peak positions during the CIT.

A domain-wall model has previously been suggested[46] for alkali-metal intercalants; in the Br_2 case, the effects are much more pronounced. Indeed we show that all of the observations can be explained by the scattering from a stripe domain phase as described in Sec. IV A. For the moment, we concentrate on the peak positions predicted by Eq. (20). All of the peak shifts are consistent with the choice $p=\frac{7}{2}$.

For example, the major and minor peaks shown in Fig. 12(a) around Br(1,5,0) in the incommensurate phase can be labeled as [1,(5,1),0] and [1,(5,2),0], respectively, using the notation introduced in Sec. IV A. Similarly the major and minor peaks shown in Fig. 12(b) around Br(0,6,0) in the incommensurate phase can be labeled as [0,(6,2),0] and [0,(6,1),0], respectively. It is of importance to note that the incommensurability ϵ is given by $\epsilon=4\pi/7L$, where L is the distance between the domain walls. Then the domain-wall density ρ is given by $\rho=7\epsilon/4\pi$. This is a very useful result since it provides for a direct measurement of the domain-wall density. The phase shift at the domain wall is $4\pi/7$, which corresponds to a displacement slip of $2b/7$ over a domain wall in real space. Good agreement is obtained between the measured and calculated shifts for $T=348.15$ K as shown in Table III, where the shifts for a number of modulation peaks are given along with their indices.

TABLE III. Measured and predicted peak shifts at $T=348.15$ K.

$[h,(k,r),l]$ peak	Measured shift (Å^{-1})	Calculated shift (Å^{-1})
[0,(4,1),0]	0.0048±0.0005	
[0,(10,3),0]	0.0050±0.0006	$\frac{1}{2}\epsilon=0.005$
[1,(3,1),0]	0.0045±0.0005	
[0,(6,2),0]	0.0098±0.0005	
[1,(1,0),0]	0.0098±0.0005	$\epsilon=0.010$
[2,(6,2),0]	0.0110±0.0010	
[0,(12,3),0]	0.0160±0.0020	
[1,(5,1),0]	0.0140±0.0005	$\frac{3}{2}\epsilon=0.015$
[1,(9,3),0]	0.0157±0.0020	

Figure 14 gives the shifts of the principal peak positions as a function of reduced temperature for the Br(0,4,0), Br(1,1,0), and Br(1,5,0) Bragg peaks. We have fitted the Br[1,(1,0),0] incommensurability by a power law

$$\epsilon=\epsilon_0(T/T_c-1)^{\beta}$$

as discussed in Sec. IV A; the best-fit parameters are $T_c=342.20\pm0.05$ K, $\epsilon_0(1,1,0)=0.076\pm0.011$ Å^{-1}, and $\beta=0.50\pm0.02$. By using the predictions $\epsilon_0(1,5,0)=\frac{3}{2}\epsilon_0(1,1,0)$ and $\epsilon_0(0,4,0)=\frac{1}{2}\epsilon_0(1,1,0)$ of the domain-wall model, and using the T_c and β values determined above, we have calculated the solid lines shown in Fig. 14 for Br[1,(5,1),0] and Br[0,(4,1),0] without any adjustable parameters. Clearly, the agreement for all three peaks is excellent. We emphasize that this power-law behavior holds for ϵ as small as 10% of its saturated value. Thus these data are comparable in quality to those obtained in the best studies of the model 2D second-order magnetic phase transitions.[47] The exponent $\beta=0.50\pm0.02$ agrees with the prediction $\beta=\frac{1}{2}$ of Pokrovsky and Talapov to within the errors. This experiment thence confirms this very important theoretical prediction.[3,18,21] Jaubert *et al.*[48] have also observed this square-root dependence at larger ϵ for Xe on Cu(110); however, for this system the commensurability is $p=2$ so that the CIT should, in fact, be a melting transition. In that case the peak position may not be simply related to the domain-wall density.

Figure 15 shows the incommensurability of the Br[1,(1,0),0] peak in a larger temperature range. It is notable that the power-law fit with $\beta=0.50\pm0.02$ starts deviating from the experimental points around 348 K and ϵ reaches its saturation value at about 355 K. This behavior is expected because in the calculation of $\beta=\frac{1}{2}$ the repulsive interaction term between the domain walls is neglected. However, with increasing domain-wall density this term becomes large so that it hinders the creation of domain walls in the highly incommensurate state. At saturation, the domain walls are separated by about 130 Å, which is approximately 7.5 unit cells.

To explain the temperature dependence of the domain-wall density properly over the whole temperature range, the interaction between the domain walls should be considered along with the domain-wall crossings. The domain-wall crossings are expected to be particularly important very close to the melting transition temperature T_m because dislocation pairs may be created in this region. We note that there is no change in the positions of the Bragg peaks which have indices k that are a multiple of 7, in agreement with Eq. (20). We emphasize that all of

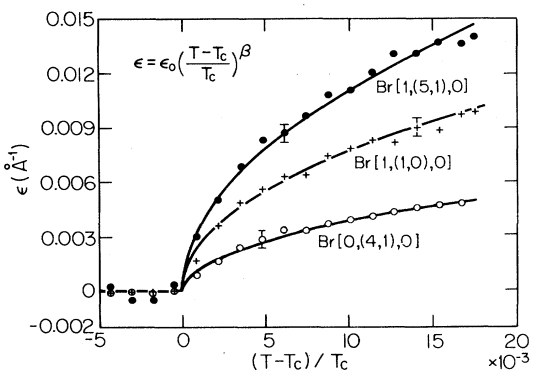

FIG. 14. Shifts of the principal peak position as a function of reduced temperature for the Br[0,(4,1),0], Br[1,(1,0),0], and Br[1,(5,1),0] peaks. Solid curves show the power-law fits as described in the text.

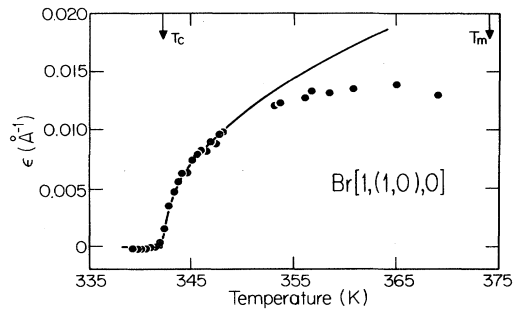

FIG. 15. Incommensurability of the principal Br[1,(1,0),0] peak in the temperature range $337<T<370$ K. Solid curve shows the power-law fit as described in the text. CIT and melting temperatures are indicated by arrows.

the observed peaks in the incommensurate phase which do not coincide with the graphite peaks are due to the domain-wall lattice; namely, they are modulation peaks.

Study of the peak intensities provides valuable information on the nature of a domain wall as suggested by Eq. (21). In this connection, Fig. 16 shows the integrated intensities of various peaks which are scaled with the observed maximum intensity in the temperature range $338 < T < 348$ K. The integrated intensities as a function of temperature all exhibit discontinuities at T_c. The dashed lines in Fig. 16 show the discontinuities expected for each peak using the structure factor given in Eq. (21). The predicted intensities of the peaks [0,(4,1),0], [1,(1,0),0], and [1,(5,1),0] are 0.93, 0.76, and 0.52, respectively, in units of their respective commensurate peak intensities. Thus the intensity discontinuity across T_c is explained well by a step-function domain wall. As shown in Figs. 16(b) and 16(c) the experimental points deviate from the predicted intensities above 343 K. This behavior, especially for the [1,(1,0),0] and [1,(5,1),0] peaks, probably arises from a temperature evolution in the power-law line shape as will be discussed in the next section. Integration of the intensity over a small q range neglects the scattering at the wings and therefore falls below the predicted intensity. Since the power-law singularity is sharpest for the [0,(4,1),0] peak, the measured and calculated intensities agree very well in this case at high temperatures.

Another test of the sharp-domain-wall model involves the comparison of the integrated intensities of various modulation peaks in the incommensurate state. For example, the fitted relative intensity of the peaks [1,(5,1),0] and [1,(5,2),0] is 1.9 compared with the calculated value [from Eq. (21)] of 1.8.

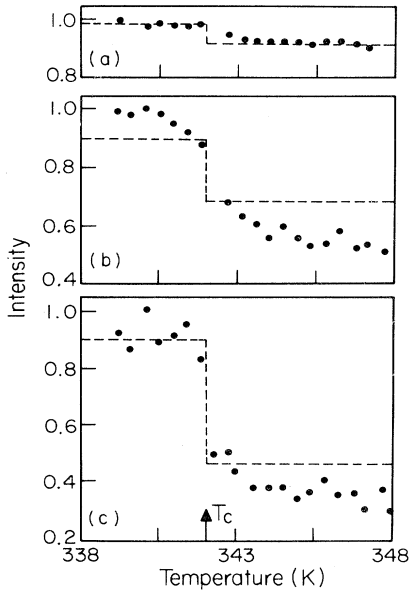

FIG. 16. (a) Integrated intensity of the peaks (a) Br[0,(4,1),0], (b) Br[1,(1,0),0], and (c) Br[1,(5,1),0] in the temperature range $338 < T < 348$ K. Dashed lines show the intensity jump at the CIT temperature predicted by the stripe domain-wall model.

We have made an explicit calculation to investigate the dependence of the structure factor on the domain-wall thickness. In this calculation we utilized the structure factor formula given in Eq. (25) by using the function $\Theta(y)$ in Eq. (10) to describe the domain wall. Our data are consistent with a domain-wall thickness of less than one unit cell. The uncertainty in the calculation of the domain-wall thickness comes from the uncertainties in the intensity measurements.

At temperatures very close to T_c the incommensurate peak coexists with the commensurate peak as shown in Fig. 17. In this figure the solid lines are all results of fits by two resolution-limited Gaussians at the commensurate and incommensurate positions. The halfwidths of the coexisting region have been measured to be 0.4 and 0.2 K for two-different single-crystal Kish graphite samples. We ascribe this to a slight distribution of chemical potentials for the domain walls. A distribution of intercalate domain sizes, defects, edge energies, and possible random interplanar interactions would give rise to a distribution of critical chemical potentials. Thus in contrast to the case of krypton on graphite where extremely broad diffraction profiles are obtained in the weakly incommensurate phase, indicating a fluid intermediate state,[14] the CIT in the Br_2 layer is a solid-solid transition. We emphasize that the CIT is completely reversible within our error limits and there is no observable hysteresis.

V. ALGEBRAIC DECAY IN THE INCOMMENSURATE Br_2 LAYER

A. Line-shape theory and analysis

In the incommensurate phase for general L the bromine system has a continuous rather than discrete symmetry. It is well known that 2D solids with continuous symmetry

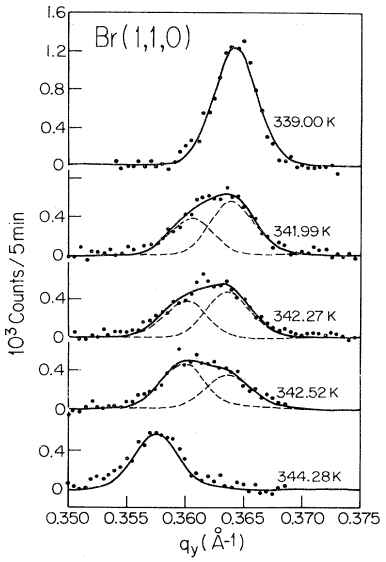

FIG. 17. Scans for the Br(1,1,0) peak showing the coexistence of the incommensurate peak with the commensurate peak at various temperatures.

exhibit power-law singularities[6,23–26] rather than true Bragg peaks. The explicit problem of a 2D lattice with 1D domain walls has been considered by a number of authors,[23–26] and their results may be readily adapted to the case of incommensurate bromine.

Specifically, if $u(x,y)$ represents a domain-wall displacement, then the part of the free energy due to the long-wavelength domain-wall Goldstone modes may be written

$$F=\frac{1}{2}\int d^2r\left[K_x\left[\frac{\partial u}{\partial x}\right]^2+K_y\left[\frac{\partial u}{\partial y}\right]^2\right], \tag{26}$$

where K_x and K_y are the elastic constants associated with, respectively, resistance to bending in the x direction due to the domain-wall stiffness and compression in the y direction due to the entropic repulsion. In the domain-wall limit, as shown by Coppersmith *et al.*[23] the concomitant structure factor may be written as

$$S_I(\vec{q})=\frac{S_0}{[K_x(q_x-G_x)^2+K_y(q_y-G_{k,r})^2]^{(1-\eta_{k,r}/2)}}, \tag{27}$$

where

$$\eta_{k,r}=\frac{1}{2\pi}k_BT(K_xK_y)^{-1/2}\left[G_{k,r}-k\frac{2\pi}{b}\right]^2 \tag{28a}$$

$$=\frac{1}{2\pi}k_BT(K_xK_y)^{-1/2}\left[\frac{2\pi}{L}\left[r-\frac{2k}{7}\right]\right]^2. \tag{28b}$$

Here S_0 is a constant, G_x is the reciprocal-lattice vector in the $\sqrt{3}$ direction, and $G_{k,r}=[h,(k,r),0]$. Schultz[26] has shown that for the peaks with the smallest incommensurability the power-law singularity exponent is given by $\eta_{G_0}=2/d^2$, where d is the number of possible sites a bromine lattice can have in the y direction.

In applying the above to the bromine system it is important to note that the phase shift at the domain wall is $4\pi/d$, not $2\pi/d$ as implicitly assumed in the theories. Thus, the minimum η is found for $G_{k,r}$ such that $r-2k/7=\pm\frac{1}{7}$; peaks exhibiting the minimum η occur, for example, around the commensurate peaks (0,4,0), (0,10,0), and (1,3,0).

The intrinsic profile $S_I(\vec{q})$ in Eq. (27) is to be convoluted with the instrumental function $R(\vec{q}-\vec{q}\,')$ to obtain the expected signal $I_1(\vec{q})$. For the graphite monochromator-spectrometer configuration the resolution function $R(\vec{q}-\vec{q}\,')$ is given by

$$R(\vec{q}-\vec{q}\,')=\frac{1}{\pi\sigma_1\sigma_2}e^{-(q_x-q_x')^2/2\sigma_1^2}e^{-(q_y-q_y')^2/2\sigma_2^2}, \tag{29}$$

where $\sigma_1=1.16\times10^{-3}$ Å^{-1} and $\sigma_2=1.37\times10^{-2}$ Å^{-1} at $k=1.45$ Å^{-1}. In scattering experiments, by changing the incoming and outgoing angles, one moves the resolution function $R(\vec{q}-\vec{q}\,')$ through reciprocal space and measures the overlap of $R(\vec{q}-\vec{q}\,')$ and the intrinsic scattering function $S_I(\vec{q}\,')$. Then the intensity is given by

$$I_1(\vec{q})=\int\int d^2q'R(\vec{q}-\vec{q}\,')S_I(\vec{q}\,'), \tag{30}$$

where the function $S_I(\vec{q}\,')$ is given in Eq. (27). We neglect the convolution of the vertical resolution function (z direction) since the scattering cross section is a Bragg rod in this direction. In addition, there are several other weakly q-dependent factors which must be included. These are the Lorentz-polarization factor C_L and the structure factor $F^{\rm calc}(\vec{q})$ as discussed in Sec. III B. Then the scattered intensity will be

$$I_2(\vec{q})=C_LF^{\rm calc}(\vec{q})I_1(\vec{q}). \tag{31}$$

In addition to the modulation peaks that we are interested in, there will also, in general, be a diffuse background due to scattering from substrate phonons, Compton scattering, scattering from the air, scattering from the Pyrex sample chamber, etc. Since this background is generally only weakly $\vec{q}$ dependent, it is modeled by a second-degree polynomial,

$$B(\vec{q})=a+bx+cx^2, \tag{32}$$

where $x\equiv|\vec{q}-\vec{q}_a|$. The parameters a, b, c, and q_a are determined by least-squares fits to a scan in the commensurate phase close to the CIT and are then fixed. It is assumed that the background parameters do not change when the sample is heated to the incommensurate state. This is a reasonable assumption because the intercalate Br_2 molecule density change during the CIT is negligible. Then the total scattering intensity will be of the form

$$I_3(\vec{q})=B(\vec{q})+C_LF^{\rm calc}(\vec{q})I_1(\vec{q}). \tag{33}$$

The scans taken in the q_x and q_y directions for a peak were analyzed using least-squares fits to the predicted line shape $I_3(\vec{q})$ given in Eq. (33). The fitting parameters consisted of the scattering amplitude S_0 and position $[h,(k,r),0]$ of each peak, the exponent $\eta_{k,r}$ and the ratio $(K_y/K_x)^{1/2}$.

B. Experimental results and discussions

At temperatures well above T_c, we have observed considerable changes in the line shapes of the incommensurate solid phase relative to those observed in the commensurate phase. In the commensurate phase, the peaks are all, to a good approximation, resolution-limited Gaussians; in the incommensurate phase the scattering in the wings increases dramatically with increasing temperature. The scattering in the wings is larger for the higher incommensurability peaks. Also, as the temperature increases, the peak intensity decreases faster for the higher incommensurability peaks. Figures 18(a) and 18(b) show the line shapes for the modulation peaks [0,(4,1),0] and [0,(6,2),0], respectively, at various temperatures. The solid lines are the results of least-squares fits to the power-law line shapes convoluted with the instrumental resolution (dashed line), as described previously. The least-squares fits yield χ^2 values less than 2. In each scan, the flat portions of the Gaussian resolution-limited curves indicate the background levels obtained from the commensurate phase. The value of the fitting parameter $\eta_{k,r}$ is given for each temperature in Fig. 18.

Although $\eta_{k,r}$ depends both on the order of the peak

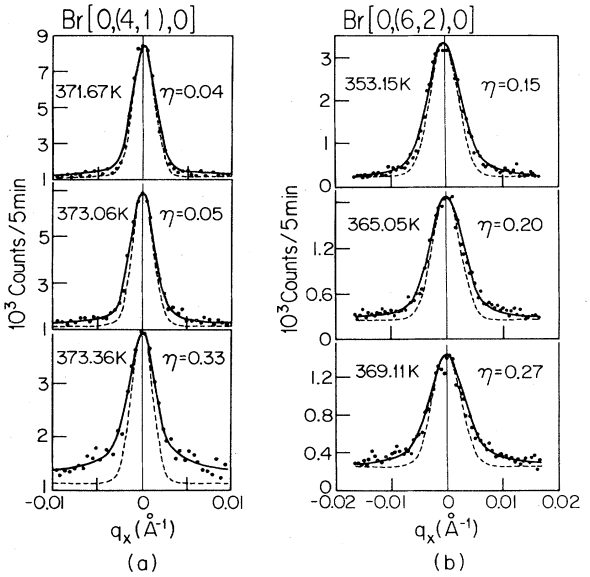

FIG. 18. Line shapes for the modulation peaks Br[0,(4,1)0] and Br[0,(6,2),0] at various temperatures in the incommensurate phase. Dashed lines show the instrument resolution function. Solid lines show the power-law line shape fits with the exponent η.

and the temperature, we find that the parameter $(K_y/K_x)^{1/2}$ remains constant within the error at 0.22 ± 0.02 for all the lines analyzed. Figure 19 shows the value of $\eta_{6,2}$ as a function of temperature for the modulation peaks Br[0,(6,2),0], Br[1,(1,0),0], and Br[0,(4,1),0]. Below 371 K, the η values for [0,(4,1),0] are not shown in Fig. 19; because these η values depend strongly on the background subtraction, they are not reliable. The accuracy of η is about 20%. As shown in Fig. 19, the η value is almost a constant in the temperature range $345<T<365$ K, but η starts to increase very rapidly as we approach the

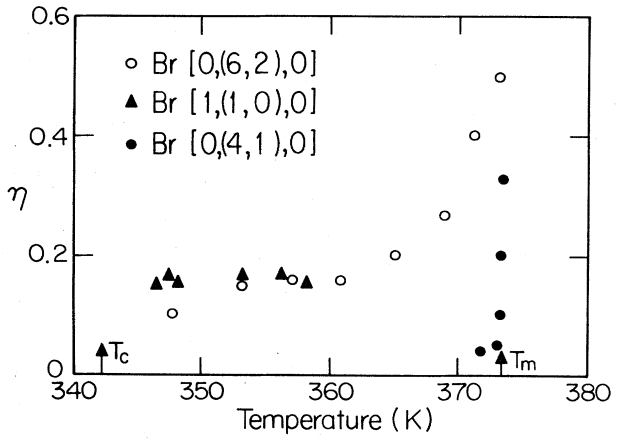

FIG. 19. Value of η as a function of temperature for the modulation peaks Br[0,(6,2),0], Br[1,(1,0),0] and Br[0,(4,1),0]. The CIT transition temperature T_c and the melting temperature T_m are indicated by arrows.

melting temperature T_m. The increase in η close to T_m may be understood qualitatively by noting that the elastic constants K_x and K_y are renormalized to smaller values near melting, thereby yielding larger η. Well below T_m for $d=7$, the value predicted for $\eta[0,(4,1),0]$ is $\eta_{G_0}=2/d^2=0.04$. Thus the formula of Eq. (28b) with $\eta\sim(r-2k/7)^2$ predicts a value of 0.16 for both $\eta[0,(6,2),0]$ and $\eta[1,(1,0),0]$. As may be seen in Fig. 19 this agrees within the errors with the best-fit values. This overall agreement is certainly very suggestive, although we have by no means demonstrated the uniqueness of this description. It is of interest to note that $\eta[0,(4,1),0]=0.33\pm0.07$ at the melting transition temperature $T_m=373.41$ K, which will be discussed in the next section. Perhaps coincidentally this η value is close to the value of $\frac{1}{4}$ predicted by Kosterlitz[49] at the dislocation-mediated melting temperature.

VI. MELTING OF THE Br_2 LAYER

To probe the nature of the melting of the bromine layer we have studied the intensities, line shapes, and linewidths of the various peaks close to the melting transition. On the fluid side of the transition we expect a Lorentzian scattering profile, corresponding to the exponential decay of the positional correlations in the intercalate layer. Then the intrinsic line shape is an anisotropic Lorentzian,

$$S(q_x,q_y)=\frac{M}{1+\xi_x^2(q_x-h_0)^2+\xi_y^2(q_y-k_0)^2}\ , \tag{34}$$

where ξ_x and ξ_y are the correlation lengths in the q_x and q_y directions, respectively. The intrinsic line shape is convoluted with the resolution function $R(\vec{q}-\vec{q}\,')$ and corrected for the form factor and the background scattering to compare with the experimental line shapes as described in detail in Sec. V A. The scans taken in the q_x and q_y directions for a peak were analyzed using least-squares fits to the predicted line shapes at the same time. The fitting parameters consisted of the amplitude M, the position $[h,(k,r),0]$ of the peak, and the correlation lengths ξ_x and ξ_y.

The line-shape parameters exhibit dramatic changes around the melting temperature. The peak intensity of the Br[0,(4,1)0] peak decreases rapidly between 372 and 374 K as shown in Fig. 20(a). The intensity is reversible upon heating and cooling within the error. It is of significance to note that the intensity of the Br[0,(4,1),0] peak remains almost constant in the temperature range $343<T<372$ K. Also shown in Fig. 20(a) is the peak intensity of the Br(2,0,0) peak as a function of temperature. It is important to emphasize that the intensity of the Br(2,0,0) peak remains constant through the melting transition. Since almost $\frac{3}{4}$ of the Br(2,0,0) intensity comes from Br_2 molecules, this peak also should exhibit a dramatic decrease similar to the Br[0,(4,1),0] peak at the melting temperature; therefore the absence of a discontinuity in the Br(2,0,0) intensity suggests a melting into an anisotropic fluid. The diffuse scattering at the point (0.005,1.455,0) Å^{-1} close to the Br[0,(4,1),0] peak is

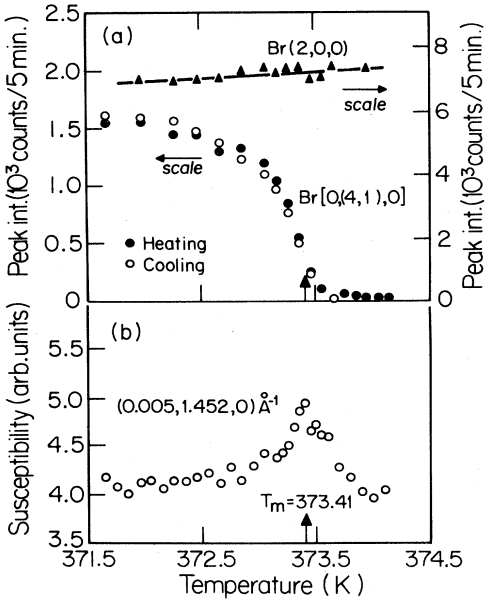

FIG. 20. (a) Peak intensities of the Br(2,0,0) and Br[0,(4,1),0] peaks as a function of temperature. (b) Susceptibility as a function of temperature at the point (0.005,1.455,0) Å^{-1} close to the Br[0,(4,1),0] peak. Peak in the susceptibility is identified with the melting transition.

shown in Fig. 20(b) as a function of temperature. The diffuse scattering is proportional to the wave-vector-dependent susceptibility and exhibits a maximum at $T_m = 373.41 \pm 0.01$ K due to critical fluctuations. We have tentatively identified T_m as the melting transition temperature; this is consistent with the previous measurements.[11,12]

The linewidth is observed to increase rapidly and continuously above T_m, indicative of decreasing correlation lengths and a solid-fluid transition. Figures 21(a) and 21(b) show the scans through the Br[0,(4,1),0] peak in the q_x and q_y directions, respectively, at various temperatures close to T_m. The solid lines are the result of least-squares fits to anisotropic Lorentzian line shapes by using both the q_x and q_y scans taken at the same temperature. Lorentzian line shapes describe the data well above T_m as expected for a fluid phase. The line shapes for the Br(0,4,0) peak are described equally well by power-law singularities and Lorentzian profiles in the temperature range $373.1 < T < 373.5$ K. However, just below $T_m = 373.41$ K the correlation length of the Lorentzian line shape becomes larger than 4000 Å, and therefore it is probably more appropriate to describe this region as solid-like.

The best-fit parameters to a Lorentzian line shape are shown in Fig. 22 as a function of temperature in the temperature range $373.2 < T < 374.1$ K. Fitting of Lorentzians to the Br[0,(4,1),0] fluid peaks has produced different correlation lengths ξ_x and ξ_y for the sevenfold and the $\sqrt{3}$-fold directions, respectively, as shown in Fig. 22(b). Specifically at T_m, ξ_x is about 2.5 times larger than ξ_y. The ratio ξ_x/ξ_y shown in Fig. 22(c) decreases continuously with increasing temperature; indeed, around 373.8 K this ratio drops below one, exhibiting opposite anisotropy from that very near T_m. This apparent crossover in the anisotropy is suggestive but not conclusive, because the background subtraction may introduce large errors in the determination of the small correlation lengths. Further

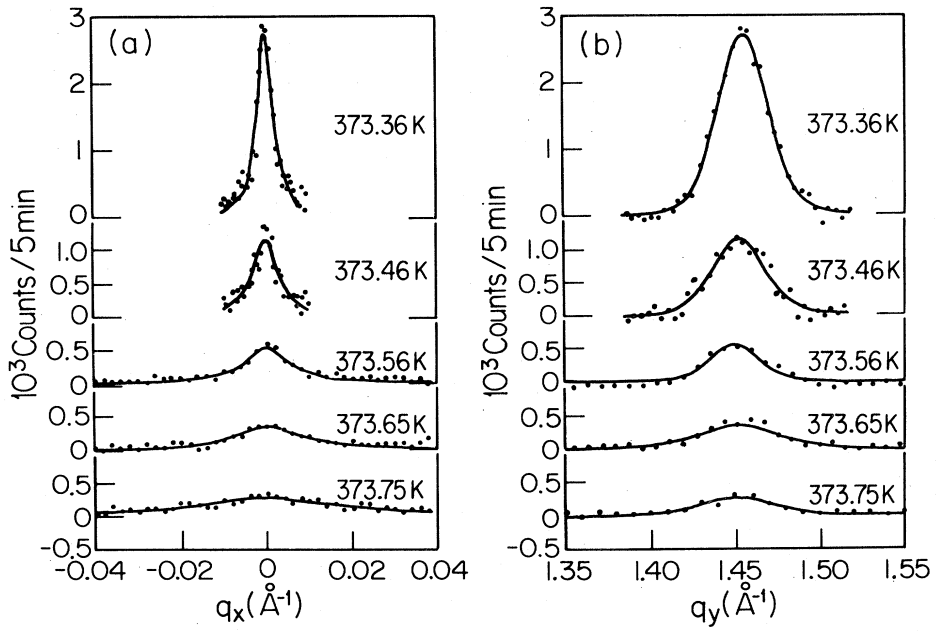

FIG. 21. Scans through the Br[0,(4,1),0] peak in the (a) q_x direction and (b) q_y direction at various temperatures close to T_m. Solid lines are the results of least-square fits to anisotropic Lorentzian line shapes by using both the q_x and q_y scans taken at the same temperature.

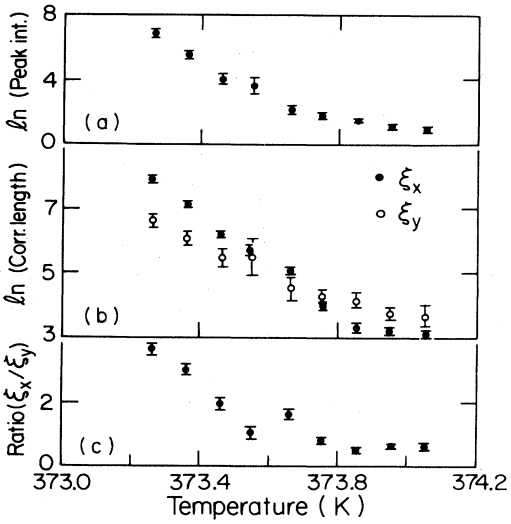

FIG. 22. Best-fit parameters to a Lorentzian line shape as a function of temperature in the temperature range $373.2 < T < 374.1$ K.

work with a more intense x-ray source is needed to characterize this novel behavior more clearly. It is clear, nevertheless, that the anomalous behavior both in the Bragg peak intensities and in the anisotropy of the correlation lengths suggests the existence of an anisotropic melting in the 2D bromine layers. This raises the exciting possibility that the "fluid" phase may actually be a 2D realization of a smectic liquid crystal as predicted theoretically.[28] However, more complete high-resolution measurements are required to establish this identification definitively.

It should also be noted that in this system dislocations involve seven domain walls annihilating at a point. Thus the characteristic length for a single dislocation is about 900 Å. It is therefore not at all clear that melting theories based on the unbinding of pairs of dislocations due to screening have any relevance to this system which can contain at most 10 dislocations in all, in a 1-μm particle. Thus it may be necessary to develop an alternative melting theory to describe this system.

VII. SUMMARY AND CONCLUSIONS

In this paper we have reported an extensive x-ray scattering study of the intercalation process, intercalant structure, and the intercalant melting and commensurate-incommensurate transitions in stage-4 bromine-intercalated graphite $C_{28}Br_2$. The intercalation process itself and the intercalant structure show a number of unexpected features. For single-crystal Kish graphite at room temperature in equilibrium with a bromine vapor of 57 Torr, the intercalation is initiated only after approximately 5.5 h and is completed after 14 h; during the entire intercalation process the bromine island size exceeds 2000 Å. One of the most dramatic results is that the material remains of very high quality even after intercalation; in particular, the intercalated graphite in-plane mosaicity is less than 0.05°. In addition, the bromine domain size exceeds 1 μm in both the commensurate and incommensurate phases. These large sizes, in turn, have made possible quite detailed studies of the intercalate phase transitions.

At room temperature, the Br_2 molecules form a centered $(\sqrt{3}\times 7)$ commensurate superlattice structure with the sevenfold axis oriented along the graphite [110] direction; each unit cell contains four Br_2 molecules. In the sample as a whole, three sets of equivalent domains are observed corresponding to the three [110] directions. From fits to eight peak intensities we deduce an in-plane structure quite close to that suggested by Eeles and Turnbull[32] and others.[33] A much more complete study is required to obtain precise positional and vibrational parameters. The Br_2 superlattice peaks take the form of rods in the c direction. At room temperature the rods exhibit a 30% sinusoidal modulation, indicating that nearest-neighbor Br_2 planes are partially correlated. Again, more detailed studies are required to establish precisely the explicit form of these correlations. When the temperature is raised to 325 K the modulation vanishes completely and the Br_2 scattering thence takes the form of true Bragg rods. This indicates that at these higher temperatures the intercalate layers are completely uncorrelated and the Br_2 layers form essentially independent 2D systems.

The Br_2 layers exhibit a particularly interesting commensurate-incommensurate transition. The graphite plane is very rigid, and therefore the in-plane unit cell does not change much with varying temperature. The Br_2 plane, on the other hand, is very soft and anharmonic. The concomitant difference in thermal expansion causes the Br_2 planes to undergo a CIT with increasing temperature; the scattering in the incommensurate phase demonstrates clearly that the Br_2 molecules predominantly occupy commensurate sites with the thermal expansion being accommodated by shifts from one sublattice to another in the sevenfold direction. This, in turn, means that the CIT and the incommensurate phase in general should be well described by a domain-wall model.

A detailed theory for a 1D CIT in a 2D lattice has been given by Pokrovsky and Talapov.[21] They predict that the domain-wall density and hence the incommensurability should initially rise as $(T-T_C)^{1/2}$ but should saturate as the domain-wall density increases. We observe just this behavior. It is found, in addition, that the incommensurate peak position and intensities are well described by a sharp-domain-wall model with domain-wall widths less than one unit cell and with a displacement at the walls of $2b/7$, where b is the lattice constant in the sevenfold direction.

Because of the continuous symmetry in the incommensurate phase the Br$[h,(k,r),0]$ peaks with $r-2k/7\neq 0$ are expected to have the form of power-law singularities rather than true Bragg peaks. We find that the Bragg profiles in the incommensurate phase do indeed exhibit extended tails. The data thence may be fitted quite well to the power-law form in Eq. (27). This description, however, is by no means unique so that the fits can only be considered as a demonstration of consistency. It is interesting to note

that $(K_y/K_x)^{1/2}$ is a constant within the error for all the lines analyzed, and further, $\eta[0,(6,2),0]$ and $\eta[1,(1,0),0]$ both agree with the prediction of Schultz.[26] A high-resolution, high-intensity study of the Bragg profiles in the incommensurate phase using synchrotron radiation would be invaluable to probe these power-law singularity effects further.

The Br_2 layers exhibit a particularly unusual melting transition. We observe that the profiles evolve continuously from a power-law to a Lorentzian form suggesting a second-order transition. On the solid side of $T_m = 373.41 \pm 0.10$ K, the $\eta_{k,r}$ values are observed to increase drastically as T is approached. In most anisotropic systems, the length ratio is a constant; however, for the Br_2 intercalant fluid the length ratio in the sevenfold and $\sqrt{3}$ directions evolves from approximately 3 very near T_m to ≤ 1 at a temperature 0.4 K above T_m. In addition, the Br(2,0,0) peak, which involves contributions from both the Br_2 and the graphite, exhibits no measurable change through T_m; for melting into a 2D fluid this peak should have exhibited a dramatic decrease in intensity ($\sim 75\%$). This suggests that in the fluid phase, substantial order has been maintained in the $\sqrt{3}$ direction, that is, the fluid is actually a 2D analog of a 3D smectic liquid crystal. The 2D smectic, of course, is stabilized by the graphite. Melting of a 2D anisotropic solid into a 2D smectic has been predicted by Ostlund and Halperin.[28] Our study of the Br_2 melting was seriously inhibited by both intensity and resolution limitations. A much more detailed study, again using synchrotron techniques, is required before this novel melting transition will have been properly characterized. The initial results, nevertheless, are quite enticing.

Clearly, $C_{28}Br_2$ exhibits unexpectedly rich behavior. The most important feature is that this stage-4 material exhibits almost ideal 2D behavior in both the commensurate and incommensurate phases. Studies of lower-stage materials to observe possible 3D effects would be most interesting. Similarly high-resolution, high-intensity measurements of the incommensurate phase and the melting transition in $C_{28}Br_2$ are required to elucidate fully these novel phenomena. Finally, extensions of these studies to lower temperatures to observe a possible CIT due to thermal contraction would also be quite interesting.

ACKNOWLEDGMENTS

We should especially like to thank Y. Iye for providing us with the Kish graphite single crystals. We should also like to thank A. N. Berker, G. Dresselhaus, P. M. Horn, P. A. Lee, S. G. J. Mochrie, and M. Sutton for a number of helpful discussions. This work was supported by the U.S. Joint Services Electronics Program under Contract No. DAAG-29-80-C-D104 (A.R.K. and R.J.B.), and by the U.S. Air Force Office of Scientific Research under Contract No. F49620-83-C-0011 (A.E. and M.S.D.).

This work was based on a thesis submitted by one of us (A.E.) in partial fulfillment of the requirements for the degree of Doctor of Philosophy at the Massachusetts Institute of Technology.

*Present address: IBM Thomas J. Watson Research Center, Yorktown Heights, NY 10598.

[1] *Ordering in Two Dimensions,* edited by S. K. Sinha (Elsevier North-Holland, New York, 1980).

[2] For a review, see J. Villain, in *Order in Strongly Fluctuating Condensed Matter Systems,* edited by T. Riste (Plenum, New York, 1980), p. 221.

[3] V. L. Pokrovsky and A. L. Talapov, Zh. Eksp. Teor. Fiz. 78, 269 (1980) [Sov. Phys.—JETP 51, 134 (1980)].

[4] For a comprehensive review, see P. Bak, Rep. Prog. Phys. 45, 587 (1982).

[5] D. R. Nelson and B. I. Halperin, Phys. Rev. B 19, 2456 (1979).

[6] P. A. Heiney, R. J. Birgeneau, G. S. Brown, P. M. Horn, D. E. Moncton, and P. W. Stephens, Phys. Rev. Lett. 48, 104 (1982).

[7] M. D. Chinn and S. C. Fain, Phys. Rev. Lett. 39, 146 (1977).

[8] P. W. Stephens, P. Heiney, R. J. Birgeneau, and P. M. Horn, Phys. Rev. Lett. 43, 47 (1979).

[9] For an extensive review, see M. S. Dresselhaus and G. Dresselhaus, Adv. Phys. 30, 139 (1981).

[10] A. R. Kortan, A. Erbil, R. J. Birgeneau, and M. S. Dresselhaus, Phys. Rev. Lett. 49, 1427 (1982).

[11] K. K. Bardhan, J. C. Wu, and D. D. L. Chung, Synth. Metals 2, 103 (1980).

[12] A. Erbil, G. Dresselhaus, and M. S. Dresselhaus, Phys. Rev. B 25, 5451 (1982).

[13] P. M. Horn, R. J. Birgeneau, P. A. Heiney, and E. M. Hammonds, Phys. Rev. Lett. 41, 961 (1978).

[14] D. E. Moncton, P. W. Stephens, R. J. Birgeneau, P. M. Horn, and G. S. Brown, Phys. Rev. Lett. 46, 1533 (1981); 49, 1679 (1982).

[15] E. M. Hammonds, P. A. Heiney, P. W. Stephens, R. J. Birgeneau, and P. M. Horn, J. Phys. C 13, L301 (1980).

[16] F. C. Frank and J. H. Van der Merwe, Proc. R. Soc. London, Ser. A 198, 216 (1949).

[17] F. D. M. Haldane and J. Villain, J. Phys. (Paris) 42, 1673 (1981).

[18] M. E. Fisher and D. S. Fisher, Phys. Rev. B 25, 3192 (1982).

[19] W. L. McMillan, Phys. Rev. B 12, 1187 (1975).

[20] P. Bak and V. J. Emery, Phys. Rev. Lett. 36, 978 (1976).

[21] V. L. Pokrovksy and A. L. Talapov, Phys. Rev. Lett. 42, 65 (1979).

[22] C. Marti and T. Ceva, Phys. Rev. Lett. 49, 1678 (1982).

[23] S. N. Coppersmith, D. S. Fisher, B. I. Halperin, P. A. Lee, and W. F. Brinkman, Phys. Rev. B 25, 349 (1982).

[24] J. Villain and P. Bak, J. Phys. (Paris) 42, 657 (1981).

[25] F. Wegner, Z. Phys. 206, 465 (1970).

[26] H. J. Shultz, Phys. Rev. B 22, 5274 (1980).

[27] J. M. Kosterlitz and D. J. Thouless, J. Phys. C 6, 1181 (1973).

[28] S. Ostlund and B. I. Halperin, Phys. Rev. B 23, 335 (1981).

[29] T. Sasa, Y. Takahashi, and T. Mukaibo, Carbon 9, 407 (1971).

[30] D. Guérard, P. Lagrange, M. El Makrini, and A. Hérold, Carbon 16, 285 (1978).

[31] N. Kambe, M. S. Dresselhaus, G. Dresselhaus, S. Basu, A. R.

McGhie, and J. E. Fisher, Mater. Sci. Eng. 40, 1 (1979); M. S. Dresselhaus, N. Kambe, A. N. Berker, and G. Dresselhaus, Synth. Metals 2, 121 (1980).
[32]W. T. Eeles and J. A. Turnbull, Proc. R. Soc. London, Ser. A 283, 179 (1965).
[33]D. Ghosh and D. D. L. Chung, Mat. Res. Bull. 18, 727 (1983).
[34]S. Y. Leung, M. S. Dresselhaus, C. Underhill, T. Krapchev, G. Dresselhuas, and B. J. Wuench, Phys. Rev. B 24, 3505 (1981).
[35]B. D. Cullity, *Elements of X-Ray Diffraction* (Addison-Wesley Reading, MA, 1956).
[36]*International Tables for X-ray Crystallography,* edited by J. A. Ibers and W. C. Hamilton (Kynock, Birmingham, England, 1974), Vol. 4.
[37]W. C. Hamilton, Acta Crystallogr. 18, 502 (1965).
[38]L. W. Finger and E. Prince, National Bureau of Standards Technical Note 854 (unpublished).
[39]R. W. G. Wyckoff, *Crystal Structures,* 2nd ed. (Interscience, New York, 1948), Vol. 1, p. 52.
[40]J. L. Feldman, E. F. Shelton, A. C. Ehrlich, D. D. Dominguez, W. T. Elam, S. B. Qadri, and F. W. Lytle, Proceedings of the 16th Biennial Conference on Carbon, San Diego, California, edited by R. J. Price and G. B. Engle, 1983, p. 209 (unpublished).
[41]J. J. Lander and J. M. Morrison, Surf. Sci. 6, 1 (1967).
[42]R. Moret, R. Comes, G. Furdin, H. Fuzellier, and F. Rousseaux, *Intercalated Graphite,* Materials Research Society Symposia Proceedings, edited by M. S. Dresselhaus, G. Dresselhaus, J. E. Fischer, and M. J. Moran, (North-Holland Elsiever, New York, 1982), Vol. 20, p. 27.
[43]S. M. Heald and E. A. Stern, Phys. Rev. B 17, 4069 (1978).
[44]A. Erbil, Ph.D. thesis, MIT, Cambridge, MA, 1983 (unpublished).
[45]S. A. Safran and D. R. Hamann, Phys. Rev. Lett. 42, 1410 (1979).
[46]R. Clarke, J. N. Gray, H. Homma, and M. J. Winokur, Phys. Rev. Lett. 47, 1407 (1981).
[47]For a review, see G. Shirane and R. J. Birgeneau, Physica (Utrecht) 86-88B, 639 (1976).
[48]M. Jaubert, A. Glachant, M. Bienfait and G. Boato, Phys. Rev. Lett. 46, 1679 (1980).
[49]J. M. Kosterlitz, J. Phys. C 7, 1046 (1974).